
Inductive Graph Representation Learning with Quantum Graph Neural Networks

Arthur M. Faria*

Ignacio F. Graña

Savvas Varsamopoulos

Pasqal SAS
Amsterdam, 1076ED Netherlands

Abstract

Quantum Graph Neural Networks (QGNNs) present a promising approach for combining quantum computing with graph-structured data processing. While classical Graph Neural Networks (GNNs) are renowned for their scalability and robustness, existing QGNNs often lack flexibility due to graph-specific quantum circuit designs, limiting their applicability to a narrower range of graph-structured problems, falling short of real-world scenarios. To address these limitations, we propose a versatile QGNN framework inspired by the classical GraphSAGE approach, utilizing quantum models as aggregators. In this work, we integrate established techniques for inductive representation learning on graphs with parametrized quantum convolutional and pooling layers, effectively bridging classical and quantum paradigms. The convolutional layer is flexible, enabling tailored designs for specific problems. Benchmarked on a node regression task with the QM9 dataset, we demonstrate that our framework successfully models a non-trivial molecular dataset, achieving performance comparable to classical GNNs. In particular, we show that our quantum approach exhibits robust generalization across molecules with varying numbers of atoms without requiring circuit modifications, slightly outperforming classical GNNs. Furthermore, we numerically investigate the scalability of the QGNN framework. Specifically, we demonstrate the absence of barren plateaus in our architecture as the number of qubits increases, suggesting that the proposed quantum model can be extended to handle larger and more complex graph-based problems effectively.

1 Introduction

Graphs provide a versatile framework for modeling complex relationships, with applications ranging from molecular structures to social networks. Unlike traditional machine learning models such as convolutional neural networks (CNNs) and feedforward neural networks (NNs), graph neural networks (GNNs) are specifically designed to exploit the relational structure inherent in graph data. This unique capability enables GNNs to excel in tasks such as node classification, link prediction, and graph regression, where understanding the relationships between entities is as critical as understanding the entities themselves. As a result, GNNs have found widespread use across diverse domains, including social network analysis [1, 2], recommendation systems [3, 4], drug discovery [5], traffic prediction [6], and polypharmacy side effects [7, 8].

While classical GNNs have achieved remarkable success, the emergence of quantum computing introduces transformative potential for machine learning. Quantum Machine Learning (QML) harnesses principles of quantum mechanics—such as entanglement, superposition, and interference—to achieve significant, and in some cases exponential [9], speedups over classical computing for specific

*arthur.faria@pasqal.com

tasks [10, 11, 12, 13, 14]. In the context of graph-based problems, Quantum Graph Neural Networks (QGNNs) hold significant potential for addressing tasks where classical models face computational bottlenecks.

Early efforts to develop QGNNs have demonstrated promise by extending classical frameworks as Graph Convolutional Networks (GCNs) [15] to the quantum domain via digital quantum circuits [16, 17, 18, 19, 20, 21, 22]. However, despite these advancements, current QGNN frameworks still encounter challenges in scalability and generalization to unseen data. As a result, current quantum approaches struggle to address the broader challenges of real-world graph datasets, where adaptability, scalability, and generalization are crucial for success.

Present Work. To address these challenges, we propose a versatile QGNN framework for inductive node embedding, extending into the quantum realm the classical GraphSAGE approach [23]. This framework samples neighborhood nodes and employs aggregator functions to efficiently combine their feature information. By integrating node features into the learning process, it captures both the topological structure and feature distribution of neighborhoods, enabling generalization to unseen data and scalability. Building on this foundation, our QGNN incorporates a similar sampling mechanism, with quantum circuits now serving as aggregators. The circuit consists of parametrized quantum convolutional and quantum pooling layers, inspired by the Quantum Convolutional Neural Network (QCNN) architecture [24].

To rigorously evaluate the performance of our QGNN framework, we conduct node regression experiments on the QM9 dataset [25, 26]. Molecules are represented as graphs, in which the nodes are corresponding to the atoms and edges to the bonds. Our results demonstrate that the quantum model performs well on the sample data, achieving strong performance metrics. While classical GNNs consistently outperform during training, the quantum model achieves comparable or slightly superior generalization, particularly as molecular complexity increases (i.e., molecules with more atoms). This highlights the robustness of our QGNN framework, which maintains consistent generalizability even for molecules with varying numbers of atoms. Based on the results of this investigation on a non-trivial use-case, we want to motivate further exploration of similar (quantum convolutional) architectures that can potentially go beyond classically simulable problems [27].

Furthermore, we numerically investigate the scalability of the QGNN framework with respect to an increasing number of qubits. This is achieved by addressing the barren plateau problem [28, 29, 30, 31, 32], where gradients vanish exponentially, hindering optimization. Leveraging insights from QCNN research [33, 34], we adopt the same conditions to show the absence of barren plateaus in our framework. Using random input node features, we numerically confirm that the quantum circuit used as an aggregator does not exhibit barren plateaus by showing that the variance of the loss function partial derivatives scales sub-exponentially with the number of qubits. Consequently, since our QGNN employs a single QGCN as an aggregator, we confirm the absence of barren plateaus in the framework, motivating its use for further investigations on more complex graph-based data.

In summary, our work makes three key contributions:

1. We introduce a novel QGNN framework that integrates standard graph sampling strategies with quantum convolutional and quantum pooling layers.
2. We evaluate the performance of our proposed approach on a non-trivial dataset (QM9).
3. We numerically investigate the QGNN framework’s scalability by confirming the absence of barren plateaus as the number of qubits increases via the variance of the loss gradients.

The paper is structured as follows: Section 2 introduces the problem dataset and explains the node regression task we aim to investigate in this work. Section 3 reviews prior work on QGNNs, identifying their limitations and proposing how our framework addresses these challenges. Section 4 provides a foundational overview of classical GNNs, with a particular focus on the GraphSAGE approach. Section 5 details our proposed QGNN framework, including the design of the quantum circuit and a discussion of its advantages and potential benefits. Section 6 presents the numerical results for both classical and quantum models benchmarked on the QM9 dataset, comparing their performance. We also numerically confirm the absence of barren plateaus in our QGNN, suggesting that the framework is scalable and capable of handling more complex graph data. Finally, Section 7 discusses the results and provides concluding remarks.

2 Molecular Data (QM9)

The QM9 dataset [25, 26] is a standard benchmark in computational chemistry, containing a set of small organic molecules with up to 9 heavy atoms with some being carbon, oxygen, nitrogen, and fluorine. It provides geometric, energetic, electronic, and thermodynamic properties calculated using density functional theory (DFT), including atomization energies, dipole moments, and HOMO-LUMO gaps. Molecular properties such as the LUMO (Lowest Unoccupied Molecular Orbital) energy, which represents the energy level of the lowest unoccupied orbital, and the HOMO (Highest Occupied Molecular Orbital) energy, are key indicators of a molecule’s reactivity and stability. These properties are inherently molecular, meaning they describe the entire molecule rather than individual atoms.

Specifically, we focus on a node regression task, i.e., using atomic properties such as node features to predict molecular properties. In our case, we employ 11 atomic features including amongst them the atomic number, hybridization state, and partial charges to predict the LUMO energy of the molecule. In this way, node regression leverages local atomic information to infer global molecular behavior.

In this investigation, each molecule is represented as a graph, where nodes encode atomic properties, and edges only indicate connectivity between atoms. For each molecule in the QM9 dataset, we extract atom features and the adjacency matrix. However, only the atom features are used as classical input to the model, while the adjacency matrix specifies the set of atom features to be used.

3 Related Work

Quantum Graph Neural Networks have emerged as a promising approach to leverage quantum computing for graph-based learning tasks. Verdon et al. [35] introduced one of the first analog QGNN frameworks, leveraging Hamiltonian evolution for tasks such as learning quantum dynamics and graph isomorphism classification using variational Ansätze. Building on this, Henry et al. [36] extended the concept by applying quantum kernel methods to classification tasks.

In contrast to analog approaches, recent research has shifted toward digital implementations using parameterized quantum circuits (PQC) for solving graph-related problems. For instance, Beer et al. [37] developed quantum neural networks (QNNs) for graph-structured quantum data, while Skolik et al. [38] introduced QAOA-type circuits designed for weighted graphs. Additionally, hybrid quantum-classical approaches have emerged as a promising solution to address qubit limitations. Ai et al. [16] proposed a framework that decomposes large graphs into smaller subgraphs, and Zhou et al. [22] combined classical clustering with PQCs. Expanding on hybrid approaches, Tuysuz et al. [39] demonstrated a quantum-classical GNN applied to the reconstruction of the particle track, further showcasing the potential of hybrid methods.

Recent advances have been made in fully quantum graph neural network (QGNN) frameworks, but significant challenges remain. Zheng et al. [20] pioneered the development of the first Quantum Graph Convolutional Network (QGCN) circuits. In their subsequent work [21], the authors proposed a QGCN with convolutional and pooling layers, providing theoretical analysis of the model. They address the barren plateau issue during training and demonstrate promising performance on datasets for graph classification tasks. However, their approach processes the full graph in a single quantum circuit, requiring qubits to encode both the adjacency matrix, nodes and edges. This can potentially lead to increased circuit sizes even for simple graphs. For larger and more complex graphs, the circuit size increases significantly, posing substantial scalability challenges. Similar limitations are observed in Liao et al. [18], whose approach faces scalability issues due to extensive circuitry and lacks numerical benchmarking. Hu et al. [17] proposed a QGCN for semi-supervised node classification tasks, achieving promising results. However, their circuit design, based on edge representations, leads to rapidly increasing circuit depth with the number of edges, creating scalability challenges for dense graphs and potential bottlenecks during training for graphs with specific symmetries. The previous works rely on amplitude encoding to map classical feature vectors to quantum states. Ryu et al. [19] addressed node regression for molecular graphs using equivariantly diagonalizable unitary quantum graph circuits (EDU-QGCs) [40]. However, their atom-to-qubit mapping becomes computationally resource-intensive for larger molecules. Finally, Mernyei et al. [40] explored equivariant quantum graph circuits using small-scale synthetic datasets, suggesting potential scalability challenges when applied to more complex graph structures.

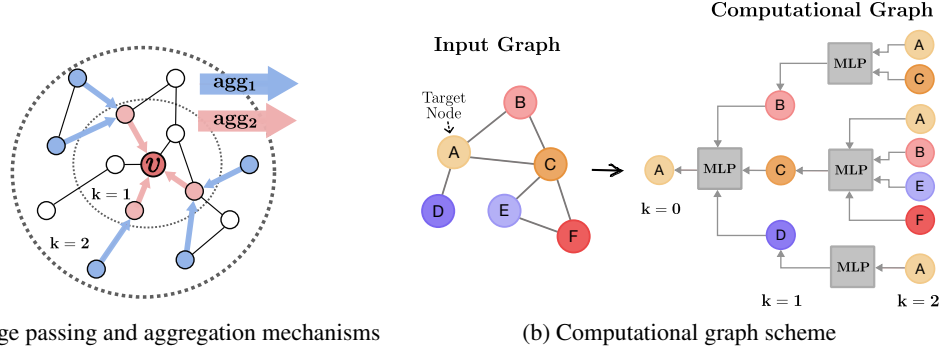


Figure 1: Illustration of the GraphSAGE framework. (a) Aggregations (agg1 and agg2) and message passing to the target node v with $k = 2$ hops. (b) Transformation of an input graph (left) into a computation graph (right), where nodes represent feature embeddings and edges indicate information flow. Gray boxes denote Multi-Layer Perceptrons (MLPs), which aggregate neighboring embeddings through modular transformations, enabling accurate node representations.

Our QGNN framework adapts GraphSAGE [23] for quantum computation, providing an efficient architecture for inductive learning on diverse graphs. By constructing the graph’s computational representation instead of directly encoding its adjacency matrix into the quantum circuit, we preserve topological features without introducing unnecessary quantum circuit overhead. The quantum circuit integrated into this framework is designed to incorporate flexible convolutional and pooling layers, enabling users to design various Ansätze. Importantly, the number of qubits depends solely on the node feature dimension, keeping the circuit architecture invariant to the number of sampled nodes and their edges. Combined with that, we employ a quantum feature map, instead of amplitude encoding, which offers rich expressivity for reasonably shallow circuit depths[41]. This framework allows classical implementations for heterogeneous graphs, as in Refs. [7, 8, 42, 43], to be extended to the quantum domain. By overcoming the limitations mentioned above, our framework provides a solid foundation for future advancements in quantum graph machine learning.

4 Classical GNN: GraphSAGE

Graph Neural Networks handle graph-structured data, where nodes represent entities and edges capture relationships between them. Unlike traditional neural networks that operate on grid-like data structures, GNNs manage flexible, interconnected structures, making them suitable for diverse applications, including social networks, molecular modeling, and knowledge graphs.

GraphSAGE is a general inductive framework that leverages node feature information to efficiently generate node embeddings. At its core are the sampling and aggregation mechanisms. Using the input graph’s adjacency matrix, the computation graph representation is constructed, preserving local graph structures. Fig. 1 provides a schematic representation of the method.

For a given depth or "hop" of the computational graph, the framework samples a fixed number of neighbors. Embeddings are dynamically generated via a modular aggregation function, producing local neighborhood embeddings for target nodes. Additionally, concatenation can be performed to incorporate the target node’s features with the aggregated neighborhood information. By stacking multiple hops, the target node embedding incorporates information from increasingly larger neighborhoods, capturing multi-hop structural information. This captures neighborhood topology, enabling scalability to large graphs and generalization to unseen data.

We now delve into the mathematical fundamentals of GraphSAGE, with a focus on the embedding generation and its propagation after the sampling and aggregation steps

4.1 Inner Workings of GraphSAGE

In GNNs, embedding generation consists of two main steps: sampling and aggregation performed by GCNs. In its layer $l = 0$, the message of target node v is $\mathbf{h}_v^{(0)} = \mathbf{x}_v$, where \mathbf{x}_v represents the input

features of v . Using the computational graph representation of the input graph, the sampling step collects features from neighboring nodes u of v . The message (MSG) generated at the GCN layer l for the neighbor u of v reads

$$\mathbf{m}_u^{(l)} = \text{MSG}^{(l)} \left(\{\mathbf{h}_u^{(l-1)}, \forall u \in \mathcal{N}(v)\} \right) \quad (1)$$

where $\mathcal{N}(v)$ represents the set of neighbors of node v . The embeddings $\mathbf{h}_u^{(l-1)}$ correspond to the representations of neighbor u from the previous layer, $l-1$. In the message-passing process, learnable parameters $\mathbf{W}^{(l)}$ (weights) and $\mathbf{B}^{(l)}$ (biases) are assigned at layer l to the neighboring nodes u and the target node v , respectively. In the aggregation step, neighbor messages are combined as follows

$$\mathbf{h}_v^{(l)} = \text{AGG}^{(l)} \left(\{\mathbf{m}_u^{(l)}, u \in \mathcal{N}(v)\}, \mathbf{m}_v^{(l)} \right), \quad (2)$$

being the aggregation (AGG) originally defined as the average of the neighboring nodes' embeddings.

In contrast, GraphSAGE introduces an intermediate step, where $\mathbf{h}_v^{(l)}$ is not updated automatically. In fact, it first enables a flexible aggregation process to generate the aggregated embedding of neighboring nodes $\mathbf{h}_{\mathcal{N}(v)}^{(l)}$, typically expressed as

$$\mathbf{h}_{\mathcal{N}(v)}^{(l)} = \text{AGG}^{(l)} \left(\{\mathbf{h}_u^{(l-1)}, \forall u \in \mathcal{N}(v)\} \right). \quad (3)$$

where AGG can be any general vector function. Common aggregation methods include MEAN, LSTM [44], or POOLING [45]. In this work, we choose the MEAN function due to its simplicity and permutation invariance. This type of aggregator computes the element-wise mean of $\{\mathbf{h}_u^{(l-1)} | u \in \mathcal{N}(v)\}$, providing a simple yet effective approach to combining neighbor information. Hence, we have $\mathbf{h}_{\mathcal{N}(v)}^{(l)} = \text{MEAN}(\{\mathbf{h}_u^{(l-1)}, \forall u \in \mathcal{N}(v)\})$, which closely resembles the aggregation procedure in the transductive GCN framework [15]. The second key feature of GraphSAGE is the concatenation of the target node's previous-layer embedding $\mathbf{h}_v^{(l-1)}$ with $\mathbf{h}_{\mathcal{N}(v)}^{(l)}$, which is not immediately done in GCNs. Now, the final embedding of v reads

$$\mathbf{h}_v^{(l)} = \sigma \left(\mathbf{W}^{(l)} \cdot \text{CONCAT} \left(\mathbf{h}_{\mathcal{N}(v)}^{(l)}, \mathbf{h}_v^{(l-1)} \right) \right). \quad (4)$$

where σ is a nonlinear activation function that enhances expressivity. The function CONCAT denotes the concatenation of embeddings. Alternatively, some GNN architectures refine this process by integrating attention mechanisms, which dynamically adjust the influence of each neighbor based on its relevance [46].

In the layer L , the final node embeddings, $\mathbf{z}_v = \mathbf{h}_v^{(L)}$ encodes both the target node's intrinsic features and its structural relationships within the graph. Hence, relying fundamentally on the features, GraphSAGE effectively captures the structural information of the graph by learning the role of a node within it. Building upon these foundations, we now extend this framework to the quantum domain, introducing the Quantum Graph Neural Network.

5 Proposed QGNN Framework

In this section, we present our QGNN framework, which integrates quantum circuits with GraphSAGE techniques to generate node embeddings. The QGNN framework comprises two key components: (1) Use of aggregation and concatenation mechanisms to generate embeddings from a node's local neighborhood features. (2) A quantum circuit that acts as a modular aggregator, combining the embeddings of connected nodes.

The first component, inspired by GraphSAGE, utilizes the adjacency matrix of the input graph to construct its computation graph representation, preserving local graph structures. This enables the

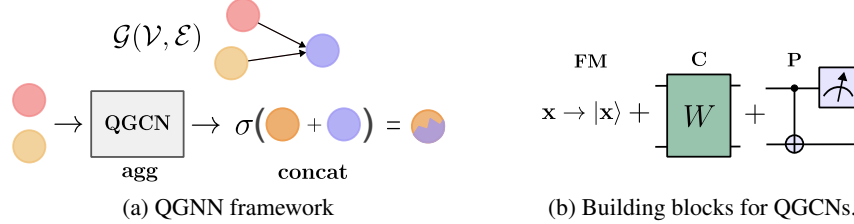


Figure 2: Schematic representation of the proposed QGNN framework and the fundamental building blocks for constructing the QGCN circuit. (a) Embedding generation process: Based on the computational graph $\mathcal{G} = (\mathcal{V}, \mathcal{E})$, node features of connected nodes (red and yellow) are sampled and input into the QGCN circuit. The QGCN aggregates these features to create neighboring node embeddings (orange), which are concatenated with the target node’s self-embedding (purple) to produce its updated embedding. To enhance expressivity, the concatenated representation undergoes a non-linear transformation σ . (b) Abstract description of operations for constructing the quantum convolutional (C) and quantum pooling (P) layers of the QGCN circuit. A feature map (FM) encodes classical inputs into an n -qubit state.

identification of connected nodes, whose features are sampled uniformly¹ and inputted into an MLP (see Fig. 1b). The second component utilizes Quantum Graph Convolutional Networks (QGCNs) as a replacement for classical MLPs to perform GraphSAGE’s aggregation. This approach leverages quantum mechanics to process node information, as illustrated in Fig. 2a. The input data is passed to the quantum circuit through a feature map, which encodes classical data into an n -qubit input state ρ_{in} , spanning an n -qubit Hilbert space \mathcal{H} . Concatenation remains unchanged, as it is a purely vector-based operation within this framework that occurs in the classical post-processing phase.

A key implication of the QGCN design is that, for nodes with feature vectors of identical dimension, the number of qubits required for encoding depends solely on this dimension. By sequentially inputting node feature vectors into the circuit, the architecture remains invariant to the number of sampled nodes and edges. Importantly, the number of qubits can be increased without altering the number of features per node, enabling additional qubits per feature for encoding. However, the minimum number of qubits must still match the number of features per node.

Together, these elements constitute our QGNN framework for node-level tasks. Fig. 2 outlines the tools and building blocks required to construct the complete QGNN. This approach extends inductive learning for graph-structured data into the quantum domain, offering a versatile and scalable framework.

5.1 The QGCN circuitry

Inspired by previous QCNN designs [24], the QGCN also alternates between quantum convolutional and quantum pooling layers.

Convolutional layers encode local graph structures by applying two qubit unitaries W_{ij} on pairs of neighboring qubits i and j . These unitaries utilize parameterized quantum gates, such as R_X and R_Z with tunable angles, which constitute the Ansatz. Controlled gates such as CZ and CNOT entangle parametrized states across qubits. This allows the quantum circuit to refine embeddings, improving expressivity while effectively capturing local structures.

Pooling layers reduces the dimensionality of quantum states while retaining essential features. This reduction simplifies data representation, decreases computational complexity, while retaining key information. Pooling is achieved by measuring a subset of qubits and using the measurement outcomes to apply classical-conditioned Pauli gates on adjacent qubits. However, the principle of deferred measurement [47] is applied as a design choice, and hence the pooling layers employ controlled operations, with (partial) measurements postponed at the end of the computation.

A generic QGCN circuit is described as a composition of quantum channels as

¹Following Ref. [23], we uniformly sample neighbors u from $\{u \in \mathcal{V} : (u, v) \in \mathcal{E}\}$.

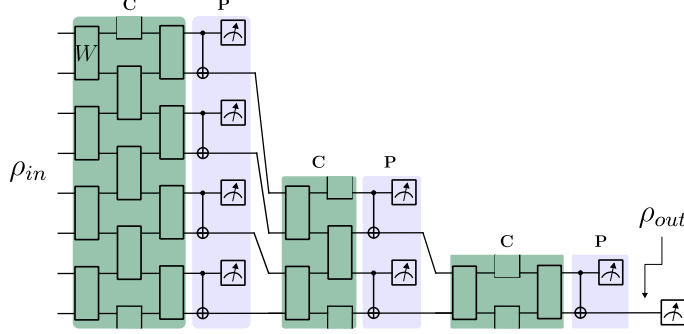


Figure 3: Schematic representation of the QGCN circuit. The QGCN takes as input an n -qubit quantum state ρ_{in} and processes it through a sequence of L alternating convolutional (C) and pooling (P) layers. In each convolutional layer, parameterized quantum gates perform unitary transformations W on pairs of neighboring qubits. The pooling layers then reduce the number of qubits by tracing out half of them between layers, preserving essential features while compressing the state space dimensionality. After the last pooling layer, the circuit produces an output state ρ_{out} , over which the expectation value of an operator \mathcal{O} is measured.

$$\Phi_{\theta, \lambda} = \bigcirc_{l=1}^L (P_l^{\lambda_l} \circ C_l^{\theta_l}), \quad (5)$$

where \circ denotes a single function composition, and $\bigcirc_{l=1}^L$ represents the composition of L functions applied sequentially. Each QGCN layer l comprises a quantum convolutional layer $C_l^{\theta_l}$ followed by a quantum pooling layer $P_l^{\lambda_l}$, with θ_l and λ_l being the convolution and pooling parameters, respectively. The alternating structure of the QGNN circuit processes and simplifies the input quantum state, starting with C_1 and ending with P_L .

The convolutional layer $C_l^{\theta_l} : \mathcal{S}(\mathcal{H}_l) \rightarrow \mathcal{S}(\mathcal{H}_l)$ preserves the size of the quantum register. It reads

$$C_l^{\theta_l}(\cdot) = \bigcirc_{j=1}^r \left(\bigotimes_{i \in S(j)} W_l^{(i, i+1)}(\theta_l) \right) (\cdot), \quad (6)$$

Each convolutional layer acts on an even number of qubits, since the unitary W_l^2 convolves a pairs of neighboring qubits $(i, i+1)$. In general, the operator W acts on pairs of adjacent qubits defined by the set $S(j) = \{(i, i+1) \mid i \equiv j \pmod{2}, 0 \leq i \leq N-2\}$, where N denotes the total number of qubits³. This construction ensures an alternating nearest-neighbor interaction pattern. The alternation is determined by the parity of j : for even j , W acts on even-indexed pairs $(0, 1), (2, 3)$, etc.; similarly, for odd values of j , the same operation is performed on odd-indexed pairs in an analogous manner. Each convolutional layer $C_l^{\theta_l}$ has an associated parameter r , representing its depth. For example, in a two-layer QGCN architecture, the depths of C_1 and C_2 are denoted as r_1 and r_2 , respectively.

The pooling layer $P_l^{\lambda_l} : \mathcal{S}(\mathcal{H}_l) \rightarrow \mathcal{S}(\mathcal{H}_{l+1})$ reduces the size of the quantum register by tracing out specific qubits, such that $\dim(\mathcal{H}_{l+1}) < \dim(\mathcal{H}_l)$, and is defined as

$$P_l^{\lambda_l}(\cdot) = \text{Tr}_i[\cdot], \quad (7)$$

where the i -qubit is traced out in the l -th layer. See Fig. 2b) for a schematic representation. The pooling layers typically discard half of the qubits at each step. The complete QGCN circuit is illustrated in Fig. 3.

We adopt a simple architecture for $C_l^{\theta_l}$ and $P_l^{\lambda_l}$, as minimal designs often achieve comparable or superior results compared to more complex counterparts [33]. In this context, the unitary W

²We also refer to W as convolutional cell.

³Qubit indexing is 0-based, i.e., $0, 1, \dots, N-1$.

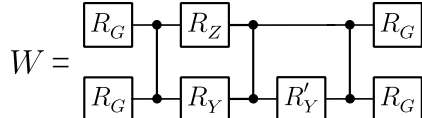


Figure 4: Schematic representation of the second convolutional unitary W , acting on two neighboring qubits. Each layer comprises of CZ gates applied to alternating qubit pairs, enclosed by parameterized general single-qubit rotations R_G . The single qubit gates: R_Z , R_Y , and, R'_Y also are parametrized with different tunable angles.

is defined as in Fig. 4, which is an optimal decomposition in the number of gates according to Ref. [48]. This minimal design employs the smallest number of quantum operations necessary to prepare any two-qubit unitary (up to a global phase), requiring only three CNOTs, three single-qubit rotation, and four general single-qubit R^G gates. We define the general rotation R^G in layer l as $R_G(\theta_l) = e^{-iX\theta_l^1/2}e^{-iZ\theta_l^2/2}e^{-iX\theta_l^3/2}$. Generally, entanglement is achieved applying non-parametrized CZ gates⁴. In the pooling layers, entanglement is followed by local measurements on \mathcal{O} , enabled by the deferred measurement principle [47]. The chosen design reduces the complexity of the QGCN circuit (5) by

$$\Phi_{\theta,\lambda} \rightarrow \Phi_{\theta}. \quad (8)$$

Hence, after the final layer L , the output state can be expressed as $\rho_{out}(\theta) = \Phi_{\theta}(\rho_{in})$. Note that a QNN can optionally be added to QGCN after its last layer, if the processing of multiple target nodes is required. The quantum circuit is finalized by measuring the observable \mathcal{O} on the remaining qubits to compute classical predictions as $\bar{y}(\theta) = \text{Tr}[\rho_{out}(\theta)\mathcal{O}]$. These predictions are then used to evaluate a loss function $\mathcal{L}_{\theta}(\bar{y}(\theta), y)$, which quantifies the discrepancy between the predicted and the true values in the training dataset. The parameters of the QCNN are then optimized by solving the task $\theta^* = \arg \min_{\theta} \mathcal{L}_{\theta}(\bar{y}(\theta), y)$. Once the optimal parameters θ^* are obtained, the model is considered trained, and its predictions are defined by the expectation values of the observable \mathcal{O} . The model is then evaluated on unseen data to assess its generalizability.

The convolutional cell W is customizable, and its definition uniquely determines the convolutional layers. In particular, QGCN layers can preserve data symmetries [49, 50, 51], making them, for example, particularly effective for symmetry-equivariant tasks. The circuit can also be extended to include QEC protocols to incorporate fault-tolerant computation [24, 52].

We now proceed to benchmark our proposed framework on the QM9 dataset, comparing its performance against its classical counterpart in predicting molecular properties.

6 Results

6.1 Implementation details

We now present the training and testing results of our QGNN framework on the QM9 dataset, comparing the performance of classical GNNs with our quantum design. Performance is evaluated using the Smooth L1 Loss and the R^2 score, with an initial focus on a small subset of molecular samples. The selected Loss is chosen for its stability and robustness to outliers, making it particularly suitable for small sample sizes with high variability. Additionally, we employ the Adam Optimizer [53] with $\beta_1 = \beta_2 = 0.9$ and a decreasing learning rate.

We train our QGNN in a supervised learning manner to predict the energy of the lowest unoccupied molecular orbital (E_{LUMO}). The algorithm processes molecules in two steps: (1) atom-level aggregation, which combines atom (or node) features with neighborhood information, and (2) molecule-level aggregation, which pools atom information into a single molecular representation. The loss function compares the predicted results with the target energy. In that way, we ensure that local and global structural information is effectively captured.

⁴In this context, CNOTs are replaced with CZs in Fig. 3.

In the proposed algorithm, we consider the following: first, we use all possible hops k for each molecule in both classical and quantum benchmarking, where k_{\max} equals the number of atoms in the molecule being processed. For instance, a 9-atom molecule undergoes 9 hops, propagating embeddings from lower-index to higher-index atoms. This restricts the computational graph to a single branch starting from the smallest-index atom. Second, this design choice eliminates the need for a final QNN layer to process multiple target nodes. This minimal approach significantly reduces computational overhead, enabling us to focus solely on benchmarking the (Q)GCNs. In addition, to avoid overfitting when aggregating the atom embeddings in both scenarios, we employ a single (Q)GCN model across the (Q)GNN framework. This ensures consistency and reduces the risk of overfitting given the small sample sizes. For more details on the algorithm, refer to App. A.

The classical GNN implemented in PYTORCH⁵[54] consists of a single hidden layers of 8 neurons, respectively. The QGCN circuit employs an 8-qubit⁶, implemented with QADENCE [55]. In this setup, the QGCN has substantially fewer tunable parameters (113) compared to its classical counterpart (209) - less than half the total parameters. Classical data from the QM9 dataset is encoded into the quantum circuit using a Fourier Feature Map [41, 56]. The QGNN comprises of three quantum convolutional layers with repetitions of $r_1 = r_2 = r_3 = 1$, and two quantum pooling layers, as defined in Eq. (7). Finally, measurements evaluate the local magnetization, defined as the expectation value of the Z Pauli operator, $\hat{M} = \sum_i \sigma_z^{(i)} / N$.

This aforementioned setup and metaparameters, along with the chosen loss and R^2 score metrics, will be employed consistently throughout the results section unless explicitly stated otherwise.

6.2 Comparison Between Classical and Quantum Models

We performed numerical simulations to compare classical GNNs with our proposed QGNNs using two cases based on molecular size and sample count, evaluated by Loss and R^2 Score. These cases include

- CASE 1: Samples of 30 molecules with up to 9 atoms,
- CASE 2: Samples of 20 molecules with up to 18 atoms.

Training uses 70% of the dataset, with 30% reserved for testing. All experiments are conducted over 300 epochs and the results are presented in Fig. 5 for each case, showing the training and testing results of the GNN and QGNN frameworks. Table 1 summarizes the final results obtained.

For Case 1, the GNN achieves superior training performance, while the QGNN demonstrates slightly better generalization on the test set. In Case 2, which includes molecules with up to twice as many atoms as Case 1, the classical model again outperforms during training, but the quantum model shows marginally better generalization. It is important to note that, despite the significant increase in the number of atoms from Case 1 to Case 2, the quantum model remains constant in depth and width (same number of input qubits), keeping the number of tunable parameters unchanged. This highlights its potential robustness in handling larger graphs without requiring design modifications.

However, while the classical GNN consistently outperforms the QGNN during training, the quantum approach exhibits faster or equal initial learning, particularly within the first 50 to 70 epochs. Furthermore, as molecular complexity increases, the quantum model maintains similar ability to generalize to unseen data despite declining training performance. This decrease, observed in both classical and quantum models, is likely due to the fixed tunable parameters for Cases 1 and 2.

The effectiveness of our framework in both training and testing highlights the potential of our QGNN to handle molecules of varying atom sizes, despite its minimal design. In addition, by benchmarking the framework on non-trivial datasets as QM9 and utilizing non-trivial Hamiltonian matrices (see Ref. [57]), we move beyond the simple datasets typically used to evaluate QML models in the literature. This motivates further exploration of such quantum convolutional architectures beyond classically simulable problems [27].

⁵For classical GNN implementations, we construct a custom GCN from scratch using PYTORCH, ensuring closer alignment with our QGNN implementation and enabling a fair classical-quantum comparison

⁶The number of qubits equals the node feature dimension plus one (accounting for concatenation with the mean of the target node’s embedding). Refer to App. A for more information.

Case	Model	# Params.	Train R ²	Train Loss	Test R ²	Test Loss
Case 1	GNN	209	0.996	0.003	0.732	0.300
	QGNN	113	0.944	0.040	0.771	0.293
Case 2	GNN	209	0.985	0.009	0.723	0.127
	QGNN	113	0.848	0.091	0.781	0.100

Table 1: Performance comparison of GNN and QGNN across Cases 1 and 2. The table highlights the number of tunable parameters, train and test R² scores, and losses for each model, emphasizing their respective results.

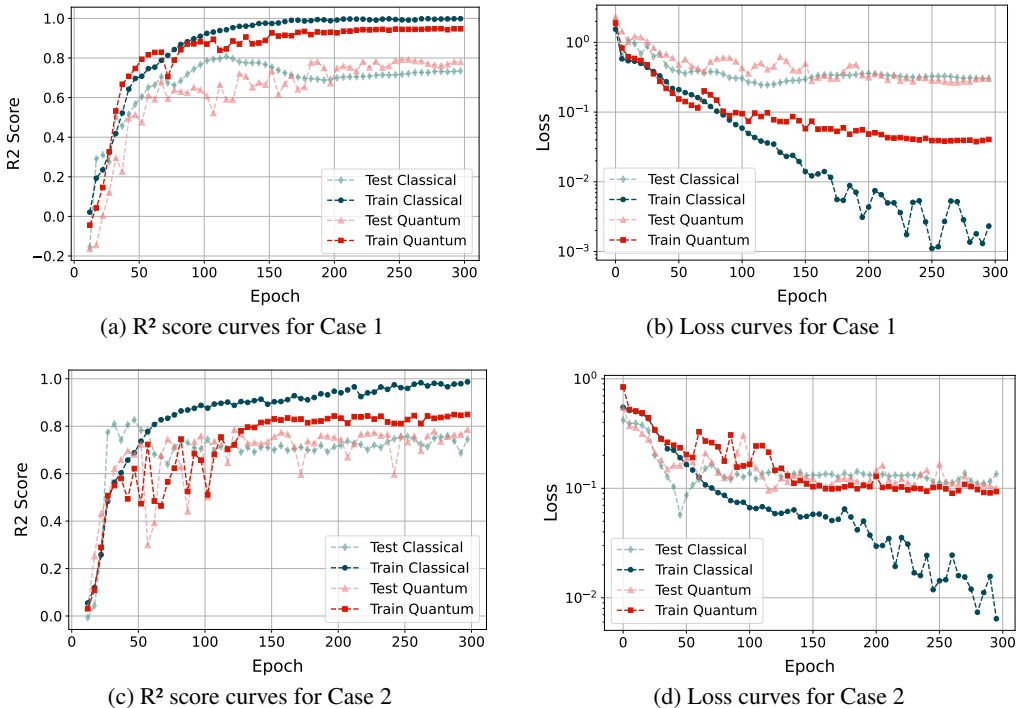


Figure 5: Comparison of training and testing performance for GNN (classical) and QGNN (quantum) models on molecules from the QM9 dataset, with all results obtained over 300 epochs. The markers are accompanied by dashed lines in their corresponding colors: circular and diamond markers distinguish the GNN’s train and test results, respectively, while square and triangular markers represent the QGNN’s train and test results. (a) and (b) present the R² score and Loss respectively for Case 1, and (c) and (d) present the R² score and Loss for Case 2.

As is clearly shown in Fig. 5, the QGNN loss for both train and test set consistently plateaus during training across all examined cases. Low model expressibility or the presence of suboptimal local minima in the loss landscape may be contributing factors that hinder the trainability of the quantum model [58, 59]. Another potential explanation for this behavior is the presence of barren plateaus, a well-documented issue in QML [33, 60]. Recent works on QCNNs [34] though indicate that barren plateaus are absent under certain conditions [33]. Since the QGCN circuitry is inspired by QCNNs, adopting similar strategies can advance QGNNs into a reliable and scalable framework for quantum graph learning.

Next, we investigate whether the previously discussed techniques can also effectively identify the absence of barren plateaus in graph machine learning problems.

6.3 Scalability and absence of barren plateaus in QGNNs

Barren plateaus [28, 29, 30, 31, 32] pose a significant challenge to the trainability of QML models [60, 61, 62, 63, 64], as they lead to an exponential decay in the gradients of the loss function. The absence of barren plateaus implies that minimizing the loss function landscape does not require exponentially high precision, allowing expectation values to be measured with polynomial precision relative to the system size. In this section, we numerically confirm the scalability of the proposed QGNN framework, as barren plateaus are absent with increasing number of qubits. This ensures continued trainability as the model scales. As previously discussed, the number of qubits in the QGCN circuit scales linearly with node feature dimensions and remains invariant to node count. Thus, changing the number of qubits does not alter the circuit.

To infer the presence of barren plateaus, we compute the loss function partial derivative $\text{Var}[\partial_{\theta_\mu} \mathcal{L}]$ —being θ_μ a variational parameter—by sampling different points in the loss landscape. According to Chebyshev’s inequality (9), the probability that the partial derivative of the cost function deviates from its mean value (which is zero) is constrained as follow [32]

$$P(|\partial_{\theta_\mu} \mathcal{L}| \geq \delta) \leq \frac{\text{Var}[\partial_{\theta_\mu} \mathcal{L}]}{\delta^2}. \quad (9)$$

where $\delta > 0$ is a positive threshold. Thus, if the variance of the loss function partial derivative decreases exponentially, the probability that the partial derivative is non-zero similarly vanishes, indicating a barren plateau.

Inspired by Ref. [34], we study the gradient scaling of our QGCN architecture under the same conditions. Specifically, we use the convolutional layer design consisting of independent (uncorrelated) local 2-designs W , as shown in Fig. 4. We also construct a correlated convolutional layer where all W ’s within each layer share the same parameters. We note this particular Ansatz significantly reduces the number of variational parameters, which may impact the model’s expressibility. Finally, the loss function is defined by local measurements, ensuring its local nature—a characteristic inherent to quantum convolutional models due to pooling layers.

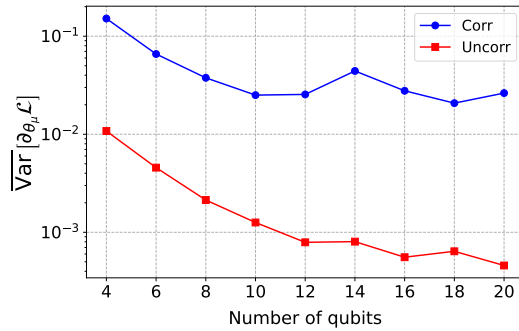


Figure 6: Average variance of the loss function partial derivatives $\overline{\text{Var}}[\partial_{\theta_\mu} \mathcal{L}]$ of the QGCN circuit. The correlated QGNN (corr) uses the same parameters for all W cells in a convolution layer, while in the uncorrelated (uncorr) all cells are independent. The variance $\text{Var}[\partial_{\theta_\mu} \mathcal{L}]$ for each variational parameter θ_μ was calculated over 200 points in the landscape.

The numerical results for the variance of the loss gradients are shown in Fig. 6. The plot displays the average variance $\overline{\text{Var}}[\partial_{\theta_\mu} \mathcal{L}] = \sum_{\mu}^N \text{Var}[\partial_{\theta_\mu} \mathcal{L}] / N$ across all N variational parameters for each QGCN circuit (correlated and uncorrelated). Unlike previous results, we use synthetic data as input node features to allow us to easily increase their dimensionality and, consequently, the number of qubits. By sampling 200 random points on the loss landscape, we compute the average variance for each parameter θ_μ , treating each number of qubit case separately. Remarkably, both the correlated and uncorrelated Ansätze suggest sub-exponential scaling of the variance, confirming the absence of barren plateaus in both models. In particular, the correlated Ansatz achieves higher variances that remain nearly constant as the number of qubits increases. This suggests that introducing correlation

in the parameters can significantly enhance the trainability of the QGNN model at scale, as large gradients are essential for efficient training.

Importantly, in benchmarking our QGNN, we employ a single QGCN circuit, so the absence of barren plateaus in the model also implies its absence in the QGNN framework. Here we conclude our analysis.

7 Conclusions

We presented a novel Quantum Graph Neural Network framework that efficiently generates node embeddings by combining inductive representation learning with quantum circuit design. Specifically, our QGNN integrates sampling and aggregation techniques from GraphSAGE, using QGCNs as aggregators. The QGCN circuit is inspired by previous QCNN designs [24], featuring convolutional and pooling layers, while maintaining high flexibility to accommodate diverse architectures. By defining the convolutional cell, the circuit is uniquely determined, enabling the construction of tailored quantum circuits for specific problems or symmetry-preserving architectures.

Benchmarking on the QM9 dataset demonstrates that the framework achieves similarly good results to the classical framework, both regarding trainability and generalization, highlighting its capability to handle non-trivial datasets. While GNNs consistently outperform during training, the QGNN achieves comparable or slightly superior generalization, particularly as molecular complexity increases. Notably, the quantum circuit architecture remains unchanged, with tunable parameters staying constant regardless of the number of nodes in a graph, showcasing good generalization and ability to handle larger graphs without requiring design modifications. Additionally, the quantum approach shows faster initial learning, indicating potential for rapid convergence.

Finally, by investigating the scalability of the QGNN, we numerically confirm the absence of barren plateaus in the proposed framework as the number of qubits increases. This suggests its potential for further improvement to tackle larger and more complex graph-based problems.

Acknowledgments

The authors thank Alexssandre de Oliveira Junior, Mehdi Djellabi, Sachin Kasture, Igor O. Sokolov, Shaheen Acheche, and Antonio Andrea Gentile for very useful discussions and comments on early drafts. A.M.F. acknowledges the project “Divide & Quantum” (P.N. 1389.20.241) of the research programme NWA-ORC (partly) financed by the Dutch Research Council (NWO). I.F.G. & S.V. acknowledge funding via “Qu&Co flow” project ID (EC): 190146292.

References

- [1] Fedor Borisuyk, Shihai He, Yunbo Ouyang, Morteza Ramezani, Peng Du, Xiaochen Hou, Chengming Jiang, Nitin Pasumarthy, Priya Bannur, Birjodh Tiwana, et al. Lignn: Graph neural networks at linkedin. *arXiv:2402.11139 [cs.LG]*, 2024.
- [2] Wenqi Fan, Yao Ma, Qing Li, Yuan He, Eric Zhao, Jiliang Tang, and Dawei Yin. Graph neural networks for social recommendation. In *The world wide web conference*, pages 417–426, 2019.
- [3] Marco De Nadai, Francesco Fabbri, Paul Giglioli, Alice Wang, Ang Li, Fabrizio Silvestri, Laura Kim, Shawn Lin, Vladan Radosavljevic, Sandeep Ghael, et al. Personalized audiobook recommendations at spotify through graph neural networks. *arXiv:2403.05185 [cs.IR]*, 2024.
- [4] Ankit Jain, Isaac Liu, Ankur Sarda, and Piero Molino. Food discovery with uber eats: Using graph learning to power recommendations. *Accessed March*, 1:2021, 2019.
- [5] Jonathan M Stokes, Kevin Yang, Kyle Swanson, Wengong Jin, Andres Cubillos-Ruiz, Nina M Donghia, Craig R MacNair, Shawn French, Lindsey A Carfrae, Zohar Bloom-Ackermann, et al. A deep learning approach to antibiotic discovery. *Cell*, 180(4):688–702, 2020.
- [6] Austin Derrow-Pinion, Jennifer She, David Wong, Oliver Lange, Todd Hester, Luis Perez, Marc Nunkesser, Seongjae Lee, Xueying Guo, Brett Wiltshire, et al. Eta prediction with graph neural networks in google maps. In *Proceedings of the 30th ACM International Conference on Information & Knowledge Management*, pages 3767–3776, 2021.
- [7] Nhat Khang Ngo, Truong Son Hy, and Risi Kondor. Modeling polypharmacy and predicting drug-drug interactions using deep generative models on multimodal graphs. *arXiv:2302.08680v1 [cs.LG]*, 2023.
- [8] Marinka Zitnik, Monica Agrawal, and Jure Leskovec. Modeling polypharmacy side effects with graph convolutional networks. *Bioinformatics*, 34(13):i457–i466, 06 2018.
- [9] Frank Arute, Kunal Arya, Ryan Babbush, Dave Bacon, Joseph C. Bardin, Rami Barends, Rupak Biswas, Sergio Boixo, Fernando G. S. L. Brandao, David A. Buell, Brian Burkett, Yu Chen, Zijun Chen, Ben Chiaro, Roberto Collins, William Courtney, Andrew Dunsworth, Edward Farhi, Brooks Foxen, Austin Fowler, Craig Gidney, Marissa Giustina, Rob Graff, Keith Guerin, Steve Habegger, Matthew P. Harrigan, Michael J. Hartmann, Alan Ho, Markus Hoffmann, Trent Huang, Travis S. Humble, Sergei V. Isakov, Evan Jeffrey, Zhang Jiang, Dvir Kafri, Kostyantyn Kechedzhi, Julian Kelly, Paul V. Klimov, Sergey Knysh, Alexander Korotkov, Fedor Kostritsa, David Landhuis, Mike Lindmark, Erik Lucero, Dmitry Lyakh, Salvatore Mandrà, Jarrod R. McClean, Matthew McEwen, Anthony Megrant, Xiao Mi, Kristel Michielsen, Masoud Mohseni, Josh Mutus, Ofer Naaman, Matthew Neeley, Charles Neill, Murphy Yuezhen Niu, Eric Ostby, Andre Petukhov, John C. Platt, Chris Quintana, Eleanor G. Rieffel, Pedram Roushan, Nicholas C. Rubin, Daniel Sank, Kevin J. Satzinger, Vadim Smelyanskiy, Kevin J. Sung, Matthew D. Trevithick, Amit Vainsencher, Benjamin Villalonga, Theodore White, Z. Jamie Yao, Ping Yeh, Adam Zalcman, Hartmut Neven, and John M. Martinis. Quantum supremacy using a programmable superconducting processor. *Nature*, 574(7779):505–510, 2019.
- [10] M Cerezo, Guillaume Verdon, Hsin-Yuan Huang, Lukasz Cincio, and Patrick J Coles. Challenges and opportunities in quantum machine learning. *Nature Computational Science*, 2022.
- [11] Patrick J Coles. Seeking quantum advantage for neural networks. *Nature Computational Science*, 1(6):389–390, 2021.
- [12] Alejandro Perdomo-Ortiz, Marcello Benedetti, John Realpe-Gómez, and Rupak Biswas. Opportunities and challenges for quantum-assisted machine learning in near-term quantum computers. *Quantum Science and Technology*, 3(3):030502, Jun 2018.
- [13] Ciliberto Carlo, Herbster Mark, Ialongo Alessandro Davide, Pontil Massimiliano, Rocchetto Andrea, Severini Simone, and Wossnig Leonard. Quantum machine learning: a classical perspective. *Proc. R. Soc. A.*, 474(20170551), 2018.
- [14] Iris Cong, Soonwon Choi, and Mikhail D. Lukin. Liu, y. and arunachalam, s. and temme, k. a. *Nat. Phys.*, 17:1013–1017, 2021.
- [15] Thomas N. Kipf and Max Welling. Semi-supervised classification with graph convolutional networks. *arXiv:1609.02907 [cs.LG]*, 2017.
- [16] Xing Ai, Zhihong Zhang, Luzhe Sun, Junchi Yan, and Edwin Hancock. Towards quantum graph neural networks: An ego-graph learning approach. *arXiv:2201.05158 [quant-ph]*, 2024.

- [17] Zhirui Hu, Jinyang Li, Zhenyu Pan, Shanglin Zhou, Lei Yang, Caiwen Ding, Omer Khan, Tong Geng, and Weiwen Jiang. On the design of quantum graph convolutional neural network in the nisq-era and beyond. In *2022 IEEE 40th International Conference on Computer Design (ICCD)*, pages 290–297, 2022.
- [18] Yidong Liao, Xiao-Ming Zhang, and Chris Ferrie. Graph neural networks on quantum computers. *arXiv:2405.17060 [quant-ph]*, 2024.
- [19] Ju-Young Ryu, Eyuel Elala, and June-Koo Kevin Rhee. Quantum graph neural network models for materials search. *Materials*, 16(12), 2023.
- [20] Jin Zheng, Qing Gao, and Yanxuan Lv. Quantum graph convolutional neural networks. *arXiv:2107.03257v1 [quant-ph]*, 2021.
- [21] Jin Zheng, Qing Gao, Maciej Ogorzałek, Jinhu Lü, and Yue Deng. A quantum spatial graph convolutional neural network model on quantum circuits. *IEEE Transactions on Neural Networks and Learning Systems*, pages 1–15, 2024.
- [22] Kaixiong Zhou, Zhenyu Zhang, Shengyuan Chen, Tianlong Chen, Xiao Huang, Zhangyang Wang, and Xia Hu. Quangcn: Noise-adaptive training for robust quantum graph convolutional networks. *arXiv:2211.07379 [quant-ph]*, 2022.
- [23] William L. Hamilton, Rex Ying, and Jure Leskovec. Inductive representation learning on large graphs. *arXiv:1706.02216v4 [cs.SI]*, 2018.
- [24] Iris Cong, Soonwon Choi, and Mikhail D. Lukin. Quantum convolutional neural networks. *Nat. Phys.*, 15:1273–1278, 2019.
- [25] Matthias Fey and Jan E. Lenssen. PyTorch Geometric: A Library for Graph Neural Networks, 2019.
- [26] Zhenqin Wu, Bharath Ramsundar, Evan N. Feinberg, Joseph Gomes, Caleb Geniesse, Aneesh S. Pappu, Karl Leswing, and Vijay Pande. Moleculenet: A benchmark for molecular machine learning. *Chem. Sci.*, 9:513–530, 2018.
- [27] Pablo Bermejo, Paolo Braccia, Manuel S. Rudolph, Zoë Holmes, Lukasz Cincio, and M. Cerezo. Quantum convolutional neural networks are (effectively) classically simulable. *arXiv:2408.12739 [quant-ph]*, 2024.
- [28] Eric R. Anschuetz and Bobak T. Kiani. Quantum variational algorithms are swamped with traps. *Nat Commun*, 13:7760, 2022.
- [29] M. Cerezo and Patrick J Coles. Higher order derivatives of quantum neural networks with barren plateaus. *Quantum Science and Technology*, 6(2):035006, 2021.
- [30] Martin Larocca, Supanut Thanasilp, Samson Wang, Kunal Sharma, Jacob Biamonte, Patrick J. Coles, Lukasz Cincio, Jarrod R. McClean, Zoë Holmes, and M. Cerezo. A review of barren plateaus in variational quantum computing. *arXiv: 2405.00781v1 [quant-ph]*, 2024.
- [31] Martin Larocca, Piotr Czarnik, Kunal Sharma, Gopikrishnan Muraleedharan, Patrick J. Coles, and M. Cerezo. Diagnosing Barren Plateaus with Tools from Quantum Optimal Control. *Quantum*, 6:824, September 2022.
- [32] Andrew Arrasmith, Zoë Holmes, M Cerezo, and Patrick J Coles. Equivalence of quantum barren plateaus to cost concentration and narrow gorges. *Quantum Science and Technology*, 7(4):045015, 2022.
- [33] M. Cerezo, Martin Larocca, Diego García-Martín, Paolo Braccia N. L. Diaz, Enrico Fontana, Manuel S. Rudolph, Pablo Bermejo, Aroosa Ijaz, Supanut Thanasilp, Eric R. Anschuetz, and Zoë Holmes. Does provable absence of barren plateaus imply classical simulability? or, why we need to rethink variational quantum computing. *arXiv:2312.09121 [quant-ph]*, 2024.
- [34] Arthur Pesah, M. Cerezo, Samson Wang, Tyler Volkoff, Andrew T. Sornborger, and Patrick J. Coles. Absence of barren plateaus in quantum convolutional neural networks. *Phys. Rev. X*, 11:041011, 2021.
- [35] Guillaume Verdon, Trevor McCourt, Enxhell Luzhnica, Vikash Singh, Stefan Leichenauer, and Jack Hidary. Quantum graph neural networks. *arXiv:1909.12264 [quant-ph]*, 2019.
- [36] Slimane Thabet, Mehdi Djellabi, Igor Sokolov, Sachin Kasture, Louis-Paul Henry, and Loïc Henriët. Quantum positional encodings for graph neural networks. *arXiv:2406.06547v1 [quant-ph]*, 2024.

- [37] Kerstin Beer, Megha Khosla, Julius Köhler, Tobias J. Osborne, and Tianqi Zhao. Quantum machine learning of graph-structured data. *Phys. Rev. A*, 108:012410, Jul 2023.
- [38] Andrea Skolik, Michele Cattelan, Sheir Yarkoni, Thomas Bäck, and Vedran Dunjko. Equivariant quantum circuits for learning on weighted graphs. *npj Quantum Information*, 9(1):47, 2023.
- [39] Cenk Tüysüz, Carla Rieger, Kristiane Novotny, Bilge Demirköz, Daniel Dobos, Karolos Potamianos, Sofia Vallecorsa, Jean-Roch Vlimant, and Richard Forster. Hybrid quantum classical graph neural networks for particle track reconstruction. *Quantum Machine Intelligence*, 3(2):1–20, 2021.
- [40] Péter Mernyei, Konstantinos Meichanetzidis, and Ismail Ilkan Ceylan. Equivariant quantum graph circuits. In *International Conference on Machine Learning*, pages 15401–15420. PMLR, 2022.
- [41] Oleksandr Kyriienko, Annie E. Paine, and Vincent E. Elfving. Solving nonlinear differential equations with differentiable quantum circuits. *Phys. Rev. A*, 103:052416, May 2021.
- [42] William L. Hamilton, Payal Bajaj, Marinka Zitnik, Dan Jurafsky, and Jure Leskovec. Embedding logical queries on knowledge graphs. *arXiv:1806.01445v4 [cs.SI]*, 2019.
- [43] Nhat Khang Ngo, Truong Son Hy, and Risi Kondor. Predicting drug-drug interactions using deep generative models on graphs. *arXiv:2209.09941 [q-bio.BM]*, 2022.
- [44] Sepp Hochreiter and Jürgen Schmidhuber. Long short-term memory. *Neural computation*, 9(8):1735–1780, 1997.
- [45] Charles R. Qi, Hao Su, Kaichun Mo, and Leonidas J. Guibas. Pointnet: Deep learning on point sets for 3d classification and segmentation. *arXiv:1612.00593 [cs.CV]*, 2017.
- [46] Petar Veličković, Guillem Cucurull, Arantxa Casanova, Adriana Romero, Pietro Liò, and Yoshua Bengio. Graph attention networks. *arXiv:1710.10903 [cs.LG]*, 2018.
- [47] Michael A. Nielsen and Isaac L. Chuang. *Quantum Computation and Quantum Information*. Cambridge University Press, 2010.
- [48] Farrokh Vatan and Colin Williams. Optimal quantum circuits for general two-qubit gates. *Phys. Rev. A*, 69:032315, 2004.
- [49] Martín Larocca, Frédéric Sauvage, Faris M. Sbahi, Guillaume Verdon, Patrick J. Coles, and M. Cerezo. Group-invariant quantum machine learning. *PRX Quantum*, 3:030341, Sep 2022.
- [50] Koki Chinzei, Quoc Hoan Tran, Kazunori Maruyama, Hirotaka Oshima, and Shintaro Sato. Splitting and parallelizing of quantum convolutional neural networks for learning translationally symmetric data. *arXiv:2306.07331 [quant-ph]*, 2023.
- [51] Quynh T. Nguyen, Louis Schatzki, Paolo Braccia Michael Ragone, Patrick J. Coles, Frederic Sauvage, Martin Larocca, and M. Cerezo. Theory for equivariant quantum neural networks. *arXiv: 2210.08566 [quant-ph]*, 2022.
- [52] Bei Zeng and D. L. Zhou. Topological and error-correcting properties for symmetry-protected topological order. *Europhysics Letters*, 113(5):56001, 2016.
- [53] Diederik P. Kingma and Jimmy Ba. Adam: A method for stochastic optimization. *arXiv:1412.6980 [cs.LG]*, 2014.
- [54] Jason Ansel, Edward Yang, Horace He, Natalia Gimelshein, Animesh Jain, Michael Voznesensky, Bin Bao, Peter Bell, David Berard, Evgeni Burovski, Geeta Chauhan, Anjali Chourdia, Will Constable, Alban Desmaison, Zachary DeVito, Elias Ellison, Will Feng, Jiong Gong, Michael Gschwind, Brian Hirsh, Sherlock Huang, Kshiteej Kalambarkar, Laurent Kirsch, Michael Lazos, Mario Lezcano, Yanbo Liang, Jason Liang, Yinghai Lu, CK Luk, Bert Maher, Yunjie Pan, Christian Puhrsch, Matthias Reso, Mark Saroufim, Marcos Yukio Siraichi, Helen Suk, Michael Suo, Phil Tillet, Eikan Wang, Xiaodong Wang, William Wen, Shunting Zhang, Xu Zhao, Keren Zhou, Richard Zou, Ajit Mathews, Gregory Chanan, Peng Wu, and Soumith Chintala. PyTorch 2: Faster Machine Learning Through Dynamic Python Bytecode Transformation and Graph Compilation. In *29th ACM International Conference on Architectural Support for Programming Languages and Operating Systems, Volume 2 (ASPLOS '24)*. ACM, April 2024.
- [55] Dominik Seitz, Niklas Heim, João Moutinho, Roland Guichard, Vytautas Abramavicius, Aleksander Wennersteen, Gert-Jan Both, Anton Quelle, Caroline Groot, Gergana Velikova, Vincent Elfving, and Mario Dagrada. Qadence: a differentiable interface for digital and analog programs. *IEEE Software*, PP:1–14, 01 2025.

- [56] Maria Schuld, Ryan Sweke, and Johannes Jakob Meyer. Effect of data encoding on the expressive power of variational quantum-machine-learning models. *Phys. Rev. A*, 103:032430, Mar 2021.
- [57] Haiyang Yu, Meng Liu, Youzhi Luo, Alex Strasser, Xiaofeng Qian, Xiaoning Qian, and Shuiwang Ji. Qh9: A quantum hamiltonian prediction benchmark for qm9 molecules. *arXiv:2306.09549 [physics.chem-ph]*, 2024.
- [58] Eric R. Anschuetz. Critical points in quantum generative models. *arXiv:2109.06957 [quant-ph]*, 2021.
- [59] Lennart Bittel and Martin Kliesch. Training variational quantum algorithms is np-hard. *Phys. Rev. Lett.*, 127:120502, 2021.
- [60] M. Cerezo, Akira Sone, Tyler Volkoff, Lukasz Cincio, and Patrick J. Coles. Cost function dependent barren plateaus in shallow parametrized quantum circuits. *Nat Commun*, 12:1791, 2021.
- [61] Jarrod R McClean, Sergio Boixo, Vadim N Smelyanskiy, Ryan Babbush, and Hartmut Neven. Barren plateaus in quantum neural network training landscapes. *Nat Commun*, 9(1):4812, 2018.
- [62] Michael Ragone, Bojko N. Bakalov, Frédéric Sauvage, Alexander F. Kemper, Carlos Ortiz Marrero, Martin Larocca, and M. Cerezo. A lie algebraic theory of barren plateaus for deep parameterized quantum circuits. *Nat Commun*, 15, 2023.
- [63] Zoë Holmes, Kunal Sharma, M. Cerezo, and Patrick J. Coles. Connecting ansatz expressibility to gradient magnitudes and barren plateaus. *PRX Quantum*, 3:010313, Jan 2022.
- [64] Pablo Bermejo, Borja Aizpurua, and Román Orús. Improving gradient methods via coordinate transformations: Applications to quantum machine learning. *Phys. Rev. Res.*, 6:023069, 2024.

A Appendix: Pseudocode for (Q)GNN algorithm on QM9 Dataset

In this appendix, we summarize the algorithm used to benchmark the performance of classical GNNs and quantum-enhanced QGNNs on the QM9 dataset. It systematically processes molecular graphs through atom-level and molecule-level operations, capturing both local and global structural information to predict molecular properties. The pseudocode 1 illustrates, at a high level, how each molecule is processed, focusing on both molecular properties (such as the target energy E_{LUMO}) and atom-level features. For each atom, an 11-dimensional feature vector is provided in PyTorch Geometric [25].

In our analysis, we employ a subset of atomic features, specifically retaining indices 0, 1, 2, 3, 4, 5, 10. These indices represent the atomic number, chirality indicator, atom degree, formal charge, radical electrons, hybridization state, and scaled atomic mass. In contrast, indices [6, 7, 8, 9] encode properties such as aromaticity, explicit hydrogen count, ring system membership, and valence. These features were excluded because their values are zero across the selected samples, providing no additional information.

Algorithm 1 (Q)GNN on QM9 dataset

Require: Batch of graphs G with adjacency matrices A , node features F , targets T , model \mathcal{M}

Ensure: $true_targets$, $predicted_targets$, and avg_loss

```
1: Initialize  $avg\_loss \leftarrow 0.0$ 
2: Initialize  $predicted\_targets \leftarrow []$ ,  $true\_targets \leftarrow []$ 
PROCESS EACH MOLECULE IN THE BATCH
3: for each molecule  $(A, F, T)$  in batch do
4:   Initialize  $previous\_output \leftarrow \mathbf{0}$ 
5:   Step1: Atom-level Aggregation and Concatenation
6:   for each node  $v$  in  $G$  do
7:     Substep 1.1: Gathering Neighboring Nodes
8:      $connected\_features \leftarrow F[A[v]]$  (if  $A[v]$  is nonzero)
9:     Substep 1.2: Concatenation
10:     $combined\_features \leftarrow \text{concat}(connected\_features, previous\_output)$ 
11:    Substep 1.3: Atom-level Aggregation
12:     $output \leftarrow \mathcal{M}(combined\_features)$ 
13:     $previous\_output \leftarrow output$ 
14:    Append  $output$  to  $atom\_outputs$ 
15:   end for
16:   Step2: Molecule-level Aggregation and Loss
17:    $molecular\_output \leftarrow \text{mean}(atom\_outputs)$ 
18:   Append  $molecular\_output$  to  $predicted\_targets$ 
19:   Append  $T$  to  $true\_targets$ 
20:    $avg\_loss \leftarrow avg\_loss + \text{criterion}(molecular\_output, T)/\text{len}(\text{batch})$ 
21: end for
22: return  $true\_targets$ ,  $predicted\_targets$ ,  $avg\_loss$ 
```

The algorithm starts with **Step 1: Atom-level Aggregation and Concatenation**, comprising three substeps. First, in Substep 1.1: *Gathering Neighboring Nodes*, each node v identifies its neighbors based on the graph’s adjacency matrix, gathering their corresponding features. Next, in Substep 1.2: *Concatenation*, these neighboring features are combined with the node’s previous output. The concatenation is done before the aggregation step, in contrast to the vanilla GNN described earlier, to ensure the tensor size remains consistent throughout the algorithm. For example, in the first iteration, the previous output is an empty vector, making this step functionally equivalent to concatenating after aggregation in the atom-level substeps. Finally, in Substep 1.3: *Atom-level Aggregation*, the concatenated features are processed by the tailored GCN to produce an output for each node. This output captures both the node’s intrinsic features and information from its neighboring atoms.

Once atom-level operations are complete, the process moves to **Step 2: Molecule-level Aggregation and Loss Calculation**. In this step, the outputs from all nodes within a molecule are aggregated using mean pooling to produce a single molecular-level output. This molecular representation is compared with the target property using a loss function, and the computed loss contributes to adjusting the model parameters. The molecular-level aggregation and loss calculation steps enable the model to capture both local and global information about the molecular structure, enhancing the tailored GCN's performance in the regression task.

In summary, the algorithm processes the graph systematically, combining atom- and molecule-level operations to capture both structural and feature-based molecular information. The algorithm described for the classical implementation also applies in the quantum context, with the classical model replaced by a quantum circuit that processes graph data through quantum convolutional and quantum pooling layers. This modification preserves the algorithm's overall structure while leveraging quantum operations to improve efficiency and expressive power.